Synthesis, Optical and Structural Properties, and Charge Carrier Dynamics of Cu-Doped ZnSe Nanocrystals
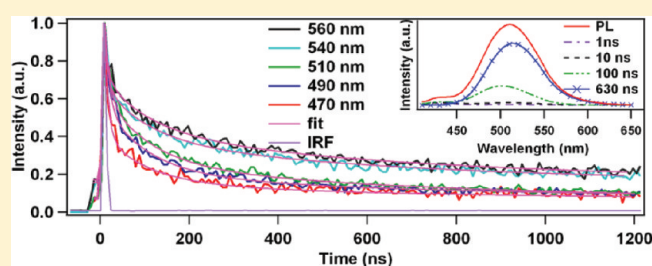
Sheraz Gul,[†] Jason K. Cooper,[†] Carley Corrado,[†] Brian Vollbrecht,[‡] Frank Bridges,[‡] Jinghua Guo,[§] and Jin Z. Zhang*,[†]

[†]Department of Chemistry and Biochemistry and [‡]Department of Physics, University of California, Santa Cruz, California 95064, United States

[§]Advanced Light Source, Lawrence Berkeley National Laboratory, Berkeley, California 94720, United States

Ⓢ Supporting Information

ABSTRACT: Stable and luminescent Cu-doped ZnSe nano-crystals (NCs) were synthesized in organic solvents with octadecylamine (ODA) as the capping ligand and characterized using a combination of optical and structural characterization techniques. Successful doping was achieved by adding Cu during the growth phase of the NCs when their size was ~4 nm. The appearance of red-shifted, intense photolumines-cence (PL) peak with doping indicates the incorpoluml of Cu in the NCs, and stability of dopant emission infers the internal doping of NCs. Extended X-ray absorption fine structure

(EXAFS) studies revealed that Cu is surrounded by four neighbors in the lattice but is very close to the NC surface and gets oxidized when NCs are precipitated from the solution. For the undoped sample, time-resolved PL studies using time-correlated single photon counting (TCSPC) reveal the luminescence decay lifetimes of about 1.1, 12, and 60 ns that we attribute to near-bandedge, shallow trap (ST) state, and deep trap (DT) state emissions, respectively. In addition to these decay components, the Cu-doped sample was found to have a long-lived component with a lifetime of 630 ns. Luminescence decay lifetimes of near-bandedge and ST state emissions were slightly shortened by doping (1 and 10 ns, respectively), suggesting that the Cu dopant competes with these states in trapping the charge carriers from the conduction band (CB) or near-bandedge states. However, the presence of Cu was found to increase the lifetime of DT states from 60 to 100 ns probably due to a decrease in coupling of electron and hole states involved in this emission upon Cu doping. Synthesis of such stable, doped samples along with a better understanding of charge carrier dynamics is significant for emerging optical applications of these NCs.

1. INTRODUCTION

Luminescent semiconductor nanocrystals (NCs) or quantum dots (QDs) have stimulated a great deal of research interest owing to their fundamentally intriguing properties resulting from quantum confinement effects and large surface-to-volume ratio,[1−9] along with their potential applications in areas including biomedical labeling, photovoltaics, and light-emitting diodes.[10−15] Their properties can be varied in a controllable manner by varying size, shape, and surface functionalization.

In particular, CdSe QDs have been studied extensively because of their absorption and emission wavelength ranges spanning much of the visible spectrum. However, the inborn toxicity of cadmium has rendered the CdSe QDs less useful, regardless of their obvious advantages.[16,17] Wide bandgap semiconductor NCs doped with transition-metal ions have developed as promising alternatives with tunable emission spanning the visible as well as near-IR spectral window. Incorporation of a small amount of dopant impurity changes the optical, magnetic, and electronic properties of host semiconductor QDs.[18−25] Some of the unique characteristics attributed to this subgroup of nanomaterials include longer excited-state lifetime, minimum self-absorption,

broad emission spectral window, and thermal stability.[25−28] These transition-metal ion-doped semiconductor NCs, such as zinc chalcogenides, can be a good alternative to the more toxic NCs for the emerging field of NC-based devices, but because of the extremely small volume of the NCs and dynamic nature of growth process, doping all NCs concurrently has been an issue to be tackled, even with powerful organometallic methods.[28−30]

In the case of ZnSe, Mn-doped NCs have been studied extensively and successfully that show stability and efficient photoluminescence ranging from 580 to 600 nm.[10,31,32] Because of similar crystal structure (zinc blende) and comparable lattice parameters of MnSe, Mn can be easily incorporated into ZnSe. However, doped NCs emitting in other regions of visible spectrum are required for some applications. Doping semiconductor NCs with Cu provides one option to fulfill this requirement, but contrary to Mn doping, serious problems have been encountered in the case of Cu doping because of different crystal

structure of copper selenide. Although some progress has been made in the recent years regarding Cu doping in this system,[25,33,34] the mechanism of Cu doping into the NCs, the nature of the Cu dopant-related emission, local structure around the dopant, and photochemical stability of the Cu-doped NCs are still unresolved issues that require further study.

Studies of charge carrier dynamics using time-resolved fluorescence measurements not only provide information about the nature of the optical transitions but also give insight into the local environment around the optically active species and provide information about how charge carriers interact with phonons and particle surface.[35,36] In addition, it is highly desirable to study the lifetimes of various decay processes involved in photoluminescence (PL) for improving device performance in applications of NCs, such as display devices, sensors, quantum cryptography, solar cells, and lasers utilizing these NCs.[1,37−40] Charge carrier dynamics studies in semiconductor NCs have proven extremely powerful in understanding fundamental properties of the particles' electronic structure that are crucially important in device applications. For instance, at the fundamental level, it is interesting to explore how the quantum confinement effects would alter the luminescent properties of dopant ions in semiconductor NCs as increase in energy level spacing has drastic effects on the rates at which excess electronic energy of an electron or hole dissipates.[13,41−43] Another factor affecting the charge carrier dynamics in NCs is the surface of particles. NCs have large percentage of surface atoms, often giving rise to surface dangling bonds and defects. Such surface defects and dangling bonds can introduce states within the bandgap of semiconductor that can strongly affect relaxation pathways of charge carriers.[44−46] Luminescence decay kinetics of Mn^{2+} doped samples has been extensively studied,[47−49] but such detailed studies of Cu-doped ZnSe are scarce and warrant further investigation.

In this work, we seek to gain some new insights regarding the doping parameters and stability of ZnSe:Cu NCs that were sufficiently stable against photo-oxidation and exhibited PL quantum yield up to 3−8% even after months. It was observed that the choice of the alkyl phosphine used to dissolve Se and the particle size at which the dopant precursor is added are very important parameters for successful doping, which requires the impurity ion to bind strongly to the surface of the host particle. As Cu ions bind strongly to only certain facets of the host NC,[29] the dopant precursor should be added when the host NCs have well-defined crystal facets that are achieved only after the particle has grown to larger sizes. The host nuclei with particle size around 4 nm are large enough to exhibit polyhedral morphology, at which point the dopant ions adsorb onto the NCs strongly enough to stay within the host lattice upon further growth, thereby achieving successful doping. NCs that were sufficiently stable against photo-oxidation and exhibited PL quantum yield up to 3% even after months were synthesized using this technique.

Furthermore, a detailed study on exciton recombination dynamics of NCs has been carried out using time-correlated single-photon counting (TCSPC). A multiexponential fit to the decay traces of undoped ZnSe sample yielded lifetimes ranging from a few nanoseconds to tens of nanoseconds, which have been attributed to near bandedge and trap state emissions. Upon doping with Cu, a new long-lived component of 630 ns appeared in addition to those observed in the case of undoped NCs, which has been attributed to the transition involving Cu specifically. Kinetics of near-bandedge and ST emissions was slightly affected by Cu doping, resulting in shortening of their lifetimes. However,

incorporation of Cu significantly affects the decay rate of DT state emission. Our findings are not only important in improving the synthesis of doped semiconductor NCs in general but also provide new insights into the charge carrier dynamics of Cu-doped ZnSe NCs specifically.

2. EXPERIMENTAL METHODS

2.1. Materials. Octadecene (ODE, 90%), zinc stearate (technical grade), tri-*n*-butylphosphine (TnBP, 99%), tributylphosphine (TBP 97%, mixture of isomers), copper acetate (98%), octadecylamine (ODA, 99%), copper acetate (99.9%), and chloroform (99.9%) were purchased from Sigma-Aldrich. Anhydrous zinc acetate (99.98%) and Se powder (<325 mesh, 99.7%) were from Alfa Aesar and Acros Organics, respectively. Methanol (99.9%), acetone (99.7%), and hexanes (99.8%) were purchased from Fisher Scientific. All chemicals were used without further purification.

2.2. Synthesis of Cu-Doped ZnSe NCs. Copper-doped ZnSe QDs were synthesized using growth-doping method similar to the one used by Peng et al.,[25] with some modification. In a typical synthesis, 0.06 g zinc stearate and 10 mL of ODE were loaded in a 50 mL three-necked flask that was then connected to Schlenk line. The mixture was evacuated up to 100 mmHg three times at room temperature and once at 90 °C for 10 min each; then, under argon flow, temperature was raised to 300 °C. Se powder (0.040 g) was dissolved in 0.40 g TBP along with 0.15 g ODA in a glovebox, and 1 mL of ODE was added to this solution. This Se solution was injected to the reaction mixture at 300 °C and was cooled to 250 °C for growth. To monitor the size of the NCs using UV−visible spectroscopy, we took small aliquots (∼0.2 mL) from the flask with a syringe and diluted them to an optical density between 0.2 and 0.3 using chloroform. When the desired particle size was reached, temperature was lowered to 200 °C, and calculated amount of copper acetate stock solution was added that was prepared by dissolving 1.074×10^{-3} g copper acetate in 1.25 g TBP. Temperature was then slowly ramped up to 220 °C and maintained for 2 h. At this temperature, slow growth continues along with the doping. To build the ZnSe shell, small amounts of 0.05 M zinc acetate solution (0.15 mL) in TBP and ODE (0.1 M solution in TBP diluted to 0.05 M with ODE) were added dropwise at regular intervals at 230 °C until stable, internally doped NCs were made, as indicated by the stability of PL. To avoid broader size distribution during growth, we added zinc and selenium solutions at regular intervals[50] except during the doping process. Undoped sample was prepared under the same conditions.

2.3. Purification of NCs. As-prepared NCs in ODE were mixed with an equal volume mixture of hexanes and methanol (1:3, v/v) by shaking vigorously and then centrifuged to get the methanol phase separated. Methanol layer was discarded, and the process was repeated two to three times. With repeated extractions, the amount of ODE gradually decreased, and that of hexanes increased with NCs being fairly soluble in this phase. To get the solid particles, after a couple of extractions, the NCs in ODE phase were precipitated using a minimum amount of acetone and recovered by centrifuging. As observed by others,[51] crashing the particles results in significant loss of PL regardless of the sample being doped or undoped. Therefore, except for XRD, ICP, and EXAFS measurements, the NCs were stored in hexanes and ODE phase obtained after repeated extractions. In this phase, NCs did not show any significant loss of PL, even after months.

B

dx.doi.org/10.1021/jp2047272 |*J. Phys. Chem. C* XXXX, XXX, 000−000

2.4. Instrumentation. The UV–visible spectra were recorded at room temperature using Hewlett-Packard 8452A diode array spectrometer. Perkin-Elmer luminescence spectrometer LS50B was used to obtain the PL and PL excitation spectra at room temperature. Low-resolution TEM measurements were performed on a JEOL model JEM-1200EX microscope at 800 KV. High-resolution TEM was performed on a Philips CM300-FEG at the National Center for Electron Microscopy at Lawrence Berkeley National Laboratory.

Cu concentrations were determined through inductively coupled plasma (ICP) measurements using a Perkin-Elmer Optima 4300DV inductively coupled plasma optical emission spectrometer (ICPOES). NCs were repeatedly purified to remove excess precursors and then dispersed in chloroform. After evaporating the chloroform, dried samples were digested in concentrated nitric acid and pumped at a rate of 1.5 mL/min into the plasma chamber. For EPR measurements, a Bruker ElexSys E500 (9.5 GHz) spectrometer, equipped with a standard TE_{102} cavity, was used. Data were collected at ~115–125K using a variable temperature control system equipped with a nitrogen vapor using cavity.

X-ray diffraction (XRD) measurements were performed on a Rigaku Americas Miniflex Plus powder diffractometer using Cu K_α ($\lambda = 1.5405$ Å) as the incident radiation. Diffraction patterns were recorded at a rate of 2° per minute with a step size of 0.04°. Sorvall RC-5C Plus centrifuge was used at 14000 rpm at room temperature to crash the NCs. FTIR measurements were carried out with a Perkin-Elmer FTIR spectrometer (spectral resolution 4 cm^{-1}).

For the EXAFS studies, ZnSe:Cu NCs were deposited on a filter paper and then encapsulated in tape; a single layer of this kind was used in the data collection process. The EXAFS data were collected at the Stanford Synchrotron Radiation Light-source (SSRL) on beamline 10–2 at 10 K using a Si (111) double monochromator, detuned 50% at 9200 eV to reduce harmonics. Small slits with a height of ~0.7 mm gave an energy resolution of 1.3 eV. The Cu K-edge data were collected in fluorescence mode, using a 13-element Ge fluorescence detector, and were reduced using standard techniques (RSXAP).[52]

Lifetime studies of the ZnSe doped and undoped systems were performed at room temperature using TCSPC. A 5W coherent Verdi-V5 (532 nm) laser was used to excite a Ti:sapphire crystal within an optical resonator cavity (Kapteyn-Murnane Laboratories, model: MTS Mini Ti:Saphire) to produce a tunable mode locked laser line between 790 and 820 nm with a frequency of 200 MHz and average power of 333 mW. The mode-locked light source was passed through a pulse picker (Conoptics, model 350-160) controlled by a Conoptics synchronous countdown (model 305), allowing for the pulse train to be set to durations ranging from 50 to 2600 ns. The pulse picked light (790 nm) was then frequency doubled by passing it through a BBO crystal that was subsequently reflected of a dichroic mirror, which was passed through a quarter wave plate and polarizer. This beam was then incident upon the sample, at which point the beam width was 2 mm. Photogenerated emission was collected at 90° with respect to the pump laser with a series of collector and focusing lenses and mirrors that guided and concentrated the signal through a 420 nm cutoff filter to remove laser light and a magic-angle polarizer before it was separated by a monochromator (Princeton Instruments SP2150i) with 0.25 nm resolution with 1200 grooves/mm and 500 nm blaze grating. The monochromatic light was focused on an avalanche photodiode (id-Quantique id100–50 single photon detection module) whose signal

was recorded with a photon counting board (Becker and Hickl, model: SPC 630) that collected in reverse stop–start mode.[53]

A number of time windows were collected to characterize adequately the wide range of time constants observed in the decay spectrum of the samples investigated and were 50, 380, and 2000 ns for individual emission wavelengths ranging from 430 to 560 nm, which were recorded every 10 nm. The undoped ZnSe QDs were probed using a 50 ns window over 4096 channels and a 380 and 1000 ns window over 1024 channels using repetition rates, which allowed the particles to recover fully for the various components measured. For the Cu-doped sample, we monitored the following time windows over the reported channels: 50 ns/4096, 380 ns/1024, and 2000 ns/256 channels. The instrumental resolutions were 0.05, 0.32, and 0.7 ns for 50, 380, and 2000 ns time windows, respectively. Data was analyzed using an IGOR Pro-based (wavemetrics) macro procedure developed in-house.

3. RESULTS AND DISCUSSION

3.1. Effect of Alkyl Phosphines on Nanocrystal Growth. Monomer activity defined as the effective monomer concentration plays a key role in NC synthesis and is profoundly affected by the ligands.[54] Alkyl phosphines are used to dissolve Se and the concentration, steric effects, and length of the alkyl chain determine the effects of alkyl phosphines on monomer reactivity. The monomer reactivity decreases with increase in ligand concentration and the strength of the bond between the monomer and ligand.[55,56] In the case of alkyl phosphines with the same number of carbon atoms, greater monomer activity was observed for those having greater steric hindrance due to alkyl chain branching. In the case of 99.9% TnBP, beyond a certain concentration (~0.5 M), the monomer phase is so stable that nucleation does not happen. However, starting with lower concentration of TnBP, nucleation does happen, but as the concentration of TnBP increases, while adding zinc acetate solution in TnBP, the particles finally disintegrate. When using Tri-iso-butylphosphine (TiBP) or mixture of isomers in which case the bonding strength to the monomer is the same as that of TnBP but owing to greater steric factor, the monomer activity is greatly enhanced, which results in better yield of NCs. Also, the NCs are found to be fairly stable at higher concentrations in the case of TiBP and mixture of isomers. This could be due to the fact that during dynamic growth of the NCs, once incorporated into the NC it is hard for the free bulky ligand to get attached to the anion and have it back into the monomer phase.

3.2. Effect of Cu-Doping on ZnSe NCs. Synthesis of transition-metal-doped II–VI semiconductor NCs has proved to be challenging. The obstacles have been reported to be due to intrinsic "self-purification" property of QDs, whereby dopants are expelled to the surface,[57,58] leading to PL quenching. However, a kinetics-based model for successful doping of semiconductor NCs has been proposed by Erwin et al.[29] On the basis of this model, adsorption strength of doping impurities on well-defined NC facets determines the doping, and binding energies of dopants are higher for Se-rich (001) facets of zinc blende structure as compared with the other crystal facets. The surface composition of the NCs can be controlled by the relative concentrations of its constituents during the nucleation and growth process. Therefore, carrying out the growth in Se-rich medium makes it possible to get NCs with Se-rich facets on the surface. As a result, all syntheses in this investigation were started with a Se:Zn ratio of 6:1. Because such well-defined facets develop after the NCs have grown up to a certain diameter, at
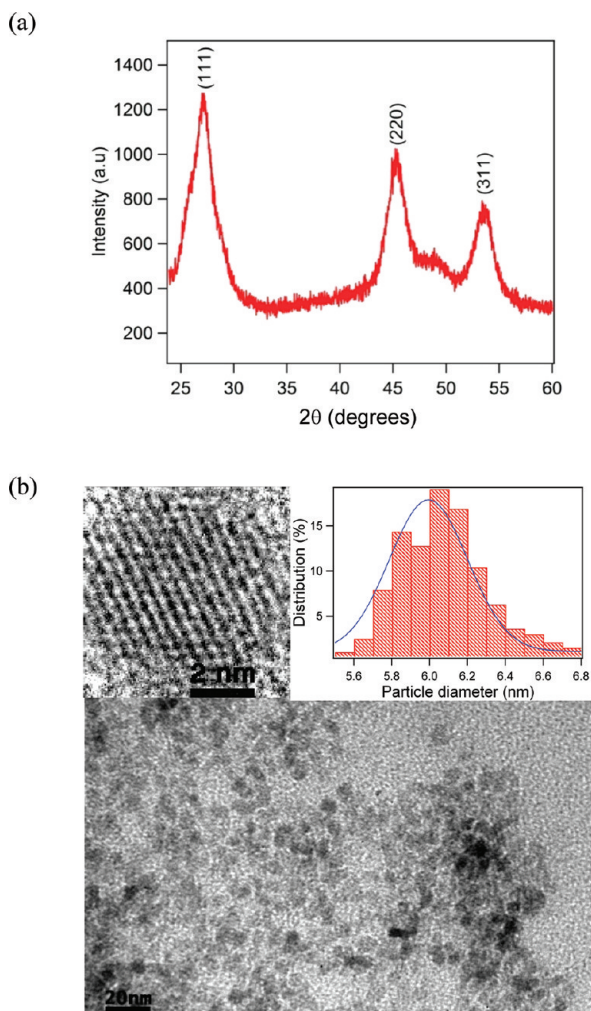
(a)

(b)

Figure 1. (a) XRD pattern of ZnSe:Cu$_{0.5\%}$ sample. (b) TEM image of NCs with inset showing HRTEM image of a single nanocrystal and the histogram.

(a)

(b)

Figure 2. (a) Average of four data scans for the ZnSe:Cu$_{0.6\%}$ sample in k-space. The data for the ZnSe:Cu$_{0.1\%}$ (not shown) have a larger amplitude and a higher signal-to-noise ratio. (b) Averaged r-space data (solid black line), fit of data to theoretical Cu−O and Cu−Se peaks (blue dots), single Cu−O peak (red line), and single Cu−Se peak (dotted magenta line) for ZnSe:Cu$_{0.1\%}$ (top panel) and ZnSe:Cu$_{0.6\%}$ (bottom panel). For the ZnSe:Cu$_{0.6\%}$, N1 = 2.060, N2 = 1.940, σ_1 = 0.0799Å, and σ_2 = 0.1049Å. For the ZnSe:Cu$_{0.1\%}$, N1 = 3.116, N2 = 0.884, σ_1 = 0.0952Å, and σ_2 = 0.0920Å.

which stage the NCs exhibit polyhedral morphology,[59] the Cu doping precursor was added after the particle size reached ∼4 nm, corresponding to an exciton peak position around 400 nm, as monitored by UV−visible absorption. Even if the dopant was added in early stage of growth, no stable PL was observed until the particle size had grown big enough to demonstrate polyhedral morphology. Also, increasing the temperature beyond 240 °C during or after the doping stage to enhance growth rate results in completely surface-doped NCs whose PL quenches quickly. Because more active zinc precursor, that is, zinc acetate dissolved in TBP, is required for growth at lower temperature, NCs were allowed to grow up to ∼4 nm at higher temperature using zinc stearate as the zinc source. This would reduce the amount of TBP required for zinc acetate solution that has to be used for growth after the addition of dopant precursor.

3.3. Structure and Composition: XRD, TEM, and ICP. Figure 1a shows the representative XRD pattern of the sample indicating a zinc blende structure. (111), (220), and (311) diffraction peaks are seen in the XRD pattern. The signal has some background from the glass substrate on which the sample was mounted. The peak broadening is an indicative of the nanocrystalline nature of sample. From the line width of (111) peak, the average crystallite size was calculated to be ∼6 nm using
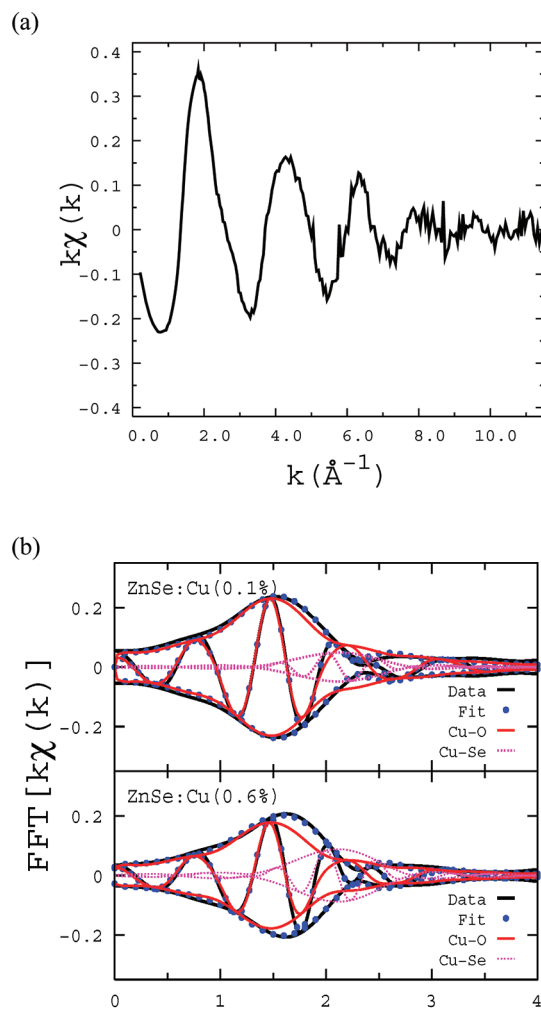
the Debye−Scherrer formula.[60] From the TEM image of ZnSe: Cu$_{0.5\%}$ sample, diameters of 150 particles were measured using the ImageJ program (distributed by NIH), and average particle size was found to be ∼6 nm with a size distribution of ∼10% (Figure 1 b). HRTEM image of single NC in the inset clearly infers the crystalline nature of QDs.

ICP measurements were performed on doped samples with varying Cu concentrations. The results showed an incorporation efficiency of almost unity with respect to the zinc incorporated. Quantitatively, this might seem a little bit higher than expected, but qualitatively these results are in agreement with observed PL attributed to Cu doping and comparable results (with 10% error) were seen from the ratios of step heights of Cu and Zn K-edges during EXAFS measurements.

3.4. Structural Characterization: EXAFS. An average of four k-space data scans for the ZnSe:Cu$_{0.6\%}$ sample is shown in Figure 2a and shows a reasonable signal-to-noise ratio out to
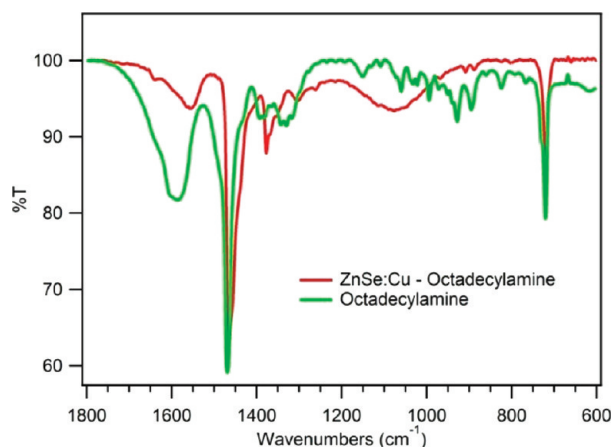
D

Figure 3. FT-IR spectra of ZnSe:Cu capped with octadecylamine as a thin film on a NaCl window (red) and octadecylamine (green) for comparative identification.

$\sim$10 Å^{-1}; for the ZnSe:Cu$_{0.1\%}$ sample, the overall amplitude is larger, and the signal-to-noise ratio is better. Figure 2b shows the r-space data obtained using a fast Fourier transform (FFT) k-range of 3.0–9.5 Å^{-1} for two samples, ZnSe:Cu$_{0.1\%}$ (top panel) and ZnSe:Cu$_{0.6\%}$ (bottom panel). The peaks in r-space correspond to shells of neighbors at different distances from the excited Cu atom. These peaks are shifted by a known amount (roughly −0.4 Å) compared with actual bond lengths.

The data in Figure 2b show a prominent peak near 1.6 Å, but in ZnSe:Cu, the first Cu−Se peak for Cu on the Zn site should occur farther out, near 2.1 Å, assuming little distortion. Therefore, an apparent shortening by $\sim$0.5 Å is unexpected and inconsistent with simple substitution. However, in CuO, Cu has four O neighbors in the first shell with almost equal bond lengths, two at 1.95 Å and two at 1.96 Å, and in r-space these peaks occur near 1.6 Å. Therefore, a visual examination of the r-space data suggests that a significant amount of oxygen has been introduced into the Cu environment in the ZnSe:Cu NCs. Theoretical Cu−O and Cu−Se single-peak EXAFS functions were generated using the known crystal structures and the FEFF8.2 code.[61] Fitting the data to a sum of these two peaks (Figure 2b, dots), with the total amplitude constrained to four neighbors and the amplitude ratio of Cu−O to Cu−Se allowed to vary, yielded a good fit for both samples. In both cases, the Cu−O amplitude was large. In these fits, the Cu−O and Cu−Se bond lengths were also allowed to vary but did not change by more than 0.01 Å, confirming the presence of oxygen in the NCs. For the ZnSe:Cu$_{0.1\%}$ sample, the Cu−O to Cu−Se amplitude ratio is roughly 3:1, whereas for ZnSe:Cu$_{0.6\%}$, the amplitude ratio is closer to 1:1, indicating a smaller relative amount of oxygen.

Because the PL of surface-doped NCs gets quenched within a few minutes,[25,33] we assume that Cu was initially present within the host NCs because PL did not show any significant decrease over a period of months if particles were not precipitated, even with a shell that was $\sim$1 nm thick. As indicated by the PL loss along with decreased solubility, crashing the NCs from solution results in considerable loss of capping ligands, which leads to surface oxidation and corrosion of NCs, as observed in CdSe,[62] where exposure to air resulted in diffusion of oxygen to deeper layers after oxidizing the surface Se. Also, the sample that shows greater Cu−O to Cu−Se amplitude ratio (3:1) was precipitated five times and suffered more loss of capping ligands as compared

with the second sample that was crashed only twice and exhibited the Cu−O to Cu−Se amplitude ratio of approximately 1:1. Alternatively, it can be argued that at lower concentrations Cu was mostly present on the surface, as reported in case of Mn-doped ZnSe[63] and Cu-doped ZnS,[64] but it requires further EXAFS investigations of the ZnSe:Cu samples in solution form before precipitating.

3.5. FTIR Analysis of Surface Ligands. Identification of the capping ligands attached to the sample after washing was achieved through use of FT-IR. In brief, a small amount of QDs dispersed in hexanes was deposited on a NaCl window and allowed to dry under N$_{2(g)}$ stream, upon which the disk was placed in the vacuum transfer chamber of a nitrogen glovebox and evacuated for 10 min. The chamber was filled with N$_{2(g)}$, and the disk was transferred to a desiccator and stored for no more than 1 h before the spectrum was collected. The resulting spectra were characteristic of an aliphatic primary amine indicated by the stretching frequencies: 1555 (NH$_2$ scissoring), 1466 and 1377 (CH$_2$ bending), 1076 (CN stretching), shoulder 738 (NH$_2$ out-of-plane bending), and 721 cm^{-1} (CH$_2$ rocking).[65] To verify the identity of the ligands, the spectrum was recorded using a sample prepared with free ODA in KBr. Both spectra have been reported in Figure 3 over the range from 600 to 1800 cm^{-1} because the NH stretching region was not useful in identification due to broadening effects and have therefore not been reported. A quick comparison of the two spectra further confirms the identity of the capping ligand as a long chain aliphatic primary amine.

3.6. Oxidation State of Copper. Although the precursors used for doping semiconductor NCs with Cu contain Cu(II), literature regarding the oxidation state of Cu in the resulting NCs is inconsistent. Whereas some have reported the existence of Cu(II),[33,34,66,67] others have argued about its incorporation as Cu(I).[64,68−71] Because Cu(II) is a d^9 system with one unpaired electron and Cu(I) being d^{10} system is diamagnetic, the EPR spectra of doped samples with different Cu amounts were taken to confirm the oxidation state of Cu within our NCs. None of the samples exhibited any detectable EPR signal (Figure S1 of the Supporting Information), indicating the presence of copper as Cu(I). This is in agreement with previous reports where no EPR signal was detected for Cu-doped semiconductor NCs, except under excitation, where paramagnetism has been observed.[72] Therefore, we believe that Cu(II) was reduced to Cu(I) in the reaction medium, as reported by Isarov et al., who have proposed the reduction of Cu(II) to Cu(I) by anions constituting the NCs.[69]

3.7. UV−visible Absorption Spectra. Successive UV−visible spectra for ZnSe:Cu$_{0.7\%}$ sample are shown in Figure 4. Given the bandgap of the bulk material being 2.69 eV (461 nm) and Bohr exciton radius of 4.5 nm,[73] the first excitonic transition at 2.99 eV (415 nm) observed in the UV−visible spectra is clearly blue-shifted and indicative of quantum confinement. After TBPSe injection, the initial growth was rapid and, within a few seconds, the first excitonic peak appeared around 380 nm, indicating the formation of NCs. Initially, the excitonic peak was broad because of a broad size distribution, but as the growth continued, the spectra evolved into narrower peaks, suggesting nearly monodisperse size distribution of NCs. Undoped and doped ZnSe NCs showed indistinguishable UV−vis spectra (Figure S2 of the Supporting Information), indicating that Cu doping has no or negligible effect on the electronic absorption of the host ZnSe NCs.

3.8. Photoluminescence. *3.8.1. Undoped ZnSe NCs.* To better understand the relevant energy levels in doped and undoped NCs, it is useful to review briefly the properties of the
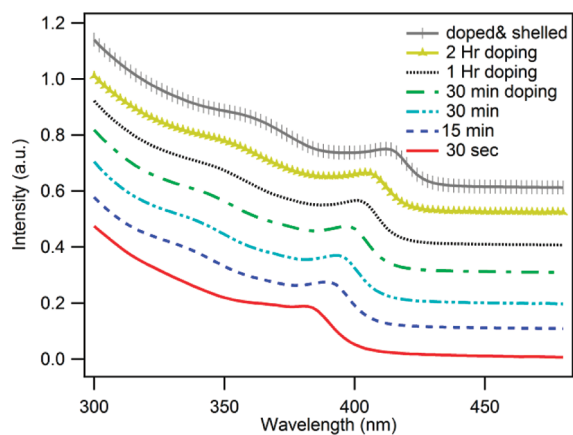
E

dx.doi.org/10.1021/jp2047272 |J. Phys. Chem. C XXXX, XXX, 000–000

Figure 4. UV–visible spectra of ZnSe:Cu$_{0.7\%}$ sample at different time intervals.
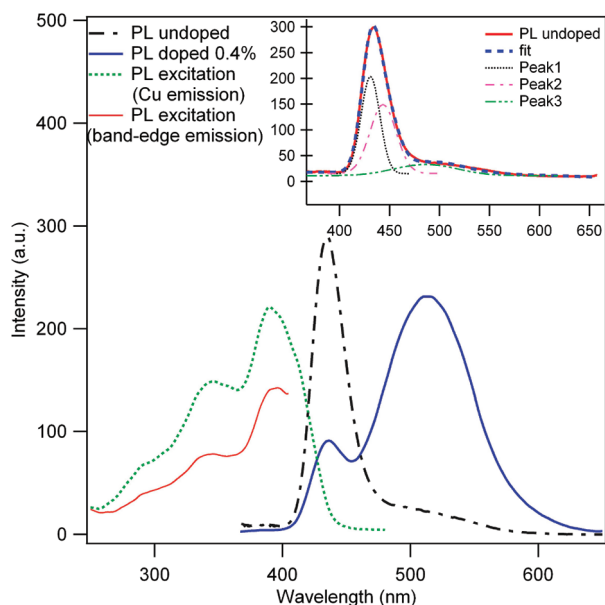

Figure 5. PL and PL excitation spectra of undoped and Cu-doped ZnSe NCs. Inset: PL spectrum of undoped sample along with the three peaks generated through fitting.

Figure 6. Proposed energy level diagram for doped and undoped sample. The blue emission at 435 nm (2.85 eV) and green Cu emission at 515 nm (2.4 eV) have been described as originating from defect and impurity-induced ST states just below the CB.

corresponding bulk system. Bulk ZnSe with a bandgap of 2.69 eV (461 nm) exhibits bandedge emission around 2.67 eV (465 nm) along with the self-activated emission involving a donor–acceptor pair (DAP).[74,75] Donor–acceptor nature of this process has been confirmed through optically detected magnetic resonance (ODMR) and time-resolved spectroscopy.[75–77] Intrinsic defects like interstitial zinc or halides that are not detectable in spectroscopic analysis could be the donors involved in self-activated emission. Recently, oxygen as an unavoidable background impurity has been reported as the donor impurity involved in self-activated emission.[78] These donor centers have been reported to exist 0.01 to 0.03 eV below the conduction band (CB), as determined by measurements of Hall coefficients of bulk samples.[79–81]

PL spectrum of undoped NC sample synthesized under the same conditions as a doped sample and excited at 390 nm is shown in Figure 5. The near-bandedge emission peak around 435 nm (2.85 eV) is asymmetric, and fitting reveals that it
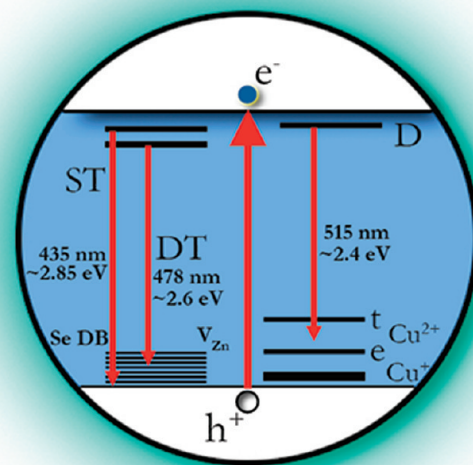
consists of two Gaussians, one peaked at 433 nm with a fwhm of 15 nm and the second one peaked at 445 nm with a fwhm of 20 nm. This might arise because of transitions involving impurity donors and ST states, respectively. The fitting is shown in the inset of Figure 5. In addition to this main band, the PL spectrum features a broad low intensity band with a maximum around 478 nm (2.6 eV), as determined by the fitting. This broad band is attributed to emission from DT states and self-activated emission comprising DAP recombination involving impurity donors and acceptors like Zn vacancies or zinc vacancy-donor-associated pairs on neighboring sites, as the sample was synthesized in Se-rich medium.

Near-bandedge emission arises from the initial excitation of valence band (VB) electron to CB from where it descends to the ST states or impurity donors and then recombines with the hole in VB or hole trap states, resulting in the emission around 435 nm. DT state emission stems from zinc vacancies or selenium dangling bonds on the surface, giving rise to states deep in the bandgap of the ZnSe NCs.[82,83] Here the photo-generated hole is immediately filled by an electron from the selenium atom with dangling bond. Subsequent emission follows after the hole migrates and finally recombines with the electron in the CB or vice versa. This emission is always broad because there would be many different selenium dangling bond species on the surface that might be singly or doubly filled. Fit generates the broad featureless region that peaks around 478 nm (Figure 5). A schematic energy level diagram describing all decay processes is shown in Figure 6.

3.8.2. Cu-doped ZnSe NCs. The spectral evolution of the PL of doped sample is shown in Figure 7. The PL spectra are similar to those observed by others previously.[25,33] The dopant precursor was not added until the host NCs had grown to a certain size (∼4 nm), where they exhibit polyhedral morphology at which stage the PL peak was ∼415 nm. After the dopant precursor was

added, the host peak started to decrease in intensity, whereas the contaminant peak increased. Complete doping took about 2 h during which time slow growth was also observed, as indicated by the movement of bandedge absorption along with a red shift of the emission band. As long as Cu ions were on the surface, the PL would decrease sharply in a few seconds; but once the host shell was grown, the PL became stable and was found to increase with time if the sample was kept under a UV light, due to photo-annealing. A digital photograph along with the corresponding PL spectra of undoped and doped NCs under UV light, with varying amounts of Cu, is shown in Figure 8, signifying the greener emission with increasing Cu amount.

With Cu-doped bulk samples, two Cu acceptor centers have been reported, one 0.7 eV above the VB involved in Cu-red emission and another 0.4 eV above the VB giving rise to Cu-green emission.[76,77,84] In the PL spectra of the NCs, the energy difference between the maxima of near-bandedge and dopant
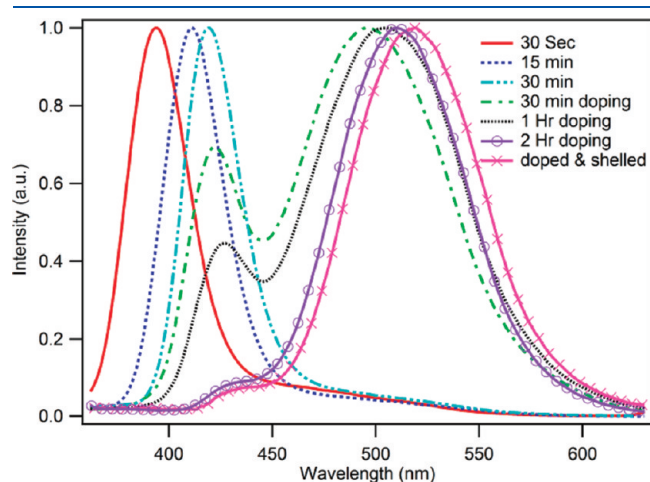

Figure 7. Normalized PL spectra before and after the addition of dopant precursor along the course of synthesis for ZnSe:Cu$_{0.7\%}$. Dopant precursor was added after the host particles have grown for 0.5 h. λ_{ex} = 335 nm when particles are really small (30 s and 15 min spectra) and λ_{ex} = 390 nm afterward.

emission was found to be ∼0.4 eV. This energy difference puts the Cu level 0.4 eV above the VB (Figure 6), indicating that the Cu emission in ZnSe:Cu NCs is analogous to the Cu green emission in the bulk material. Because of quantum confinement effects, the CB moves to higher energies, resulting in blue shifting of the green emission with decreasing particle size.

A proposed mechanism of the observed emission involves the initial excitation of a VB electron to the CB in the host ZnSe. Cu(I) ion being negatively charged with respect to the lattice then binds the hole through long-range coulomb interaction in an effective mass-like state, producing a transient Cu^{2+} acceptor state. This process involves a transition from undistorted Cu$^+$ to Jahn−Teller distorted Cu^{2+} ion, but lattice strain during this transition is not taken into account because when Cu is substituted into a tetrahedral lattice site, Jahn−Teller effect has to work against the forces maintaining the lattice, and distortion is expected to be minimized. Next, the electron in the CB moves to a ST state associated with zinc dangling bonds or impurity donors such as halides or associated oxygen, as observed in EXAFS analysis, from whereon follows the recombination of this electron with the hole-trapped d-state of Cu. This donor−acceptor recombination results in emission at 515 nm (2.4 eV).

Transient Cu^{2+} state is split into higher t and lower e levels (Figure 6), giving rise to $^2T_2$ (^2D) ground state or ^2E excited state, and both of these have the possibility to accept excited electron, which results in broadening of the dopant peak[71,85,86] that has a fwhm of ∼80 nm. The positions of neither excitonic nor the dopant emission band show any change with excitation wavelengths between 335 to 390 nm. Also, the PL excitation spectra recorded for different emission wavelengths were found to be similar. This further supports the view that broadness of emission is intrinsic and not due to heterogeneity of NCs in terms of particle size distribution. During the 2 h doping process, no zinc precursor was added that resulted in broader particle size distribution, but addition of zinc precursor during shell growth was found to make the size distribution narrower, resulting in the reduction of fwhm of dopant peak from 85 to 80 nm.

3.9. Time-Resolved Fluorescence. *3.9.1. Kinetics of the Blue Emission Band.* Fluorescence lifetimes of different decay processes
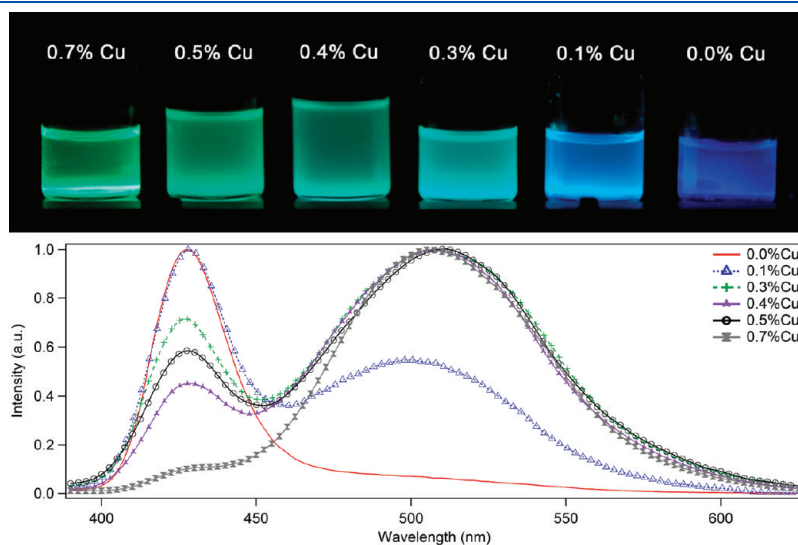

Figure 8. Digital photograph along with the PL spectra of undoped and doped ZnSe NCs, with different concentrations of Cu, under UV irradiation.
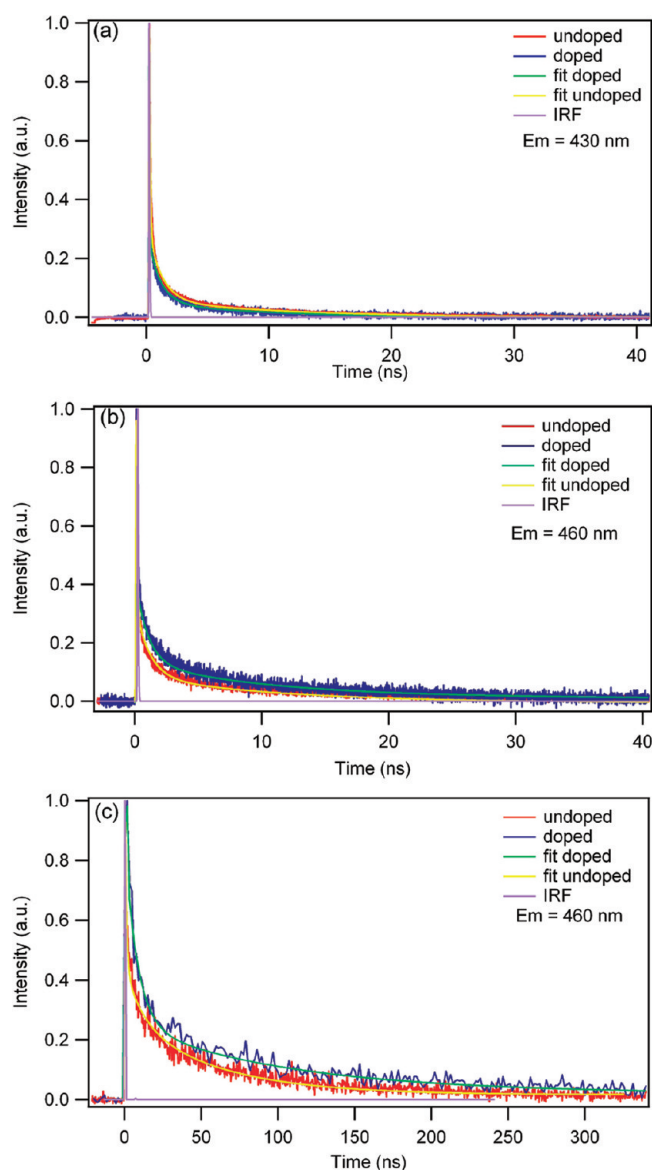
Figure 9. (a) TCSPC traces of undoped (red) and doped ZnSe:Cu$_{0.7\%}$ (blue) at 430 nm. (b) Decay collected at 460 nm for undoped (red) and doped (blue) samples with shorter time window. (c) 460 emission intensity vs time collected with a longer time sweep. Smooth lines represent the fit.

Table 1. Lifetimes for Various Decay Components in ZnSe: Cu and ZnSe NCs

sample	τ_1 (ns)	τ_2 (ns)	τ_3 (ns)	τ_4 (ns)
ZnSe:Cu	1.0 ± 0.05	10 ± 1	100 ± 10	630 ± 130
ZnSe	1.1 ± 0.05	12 ± 1	60 ± 10	

recorded at 430 nm on the short time scale (50 ns), where most of the PL comprises excitonic emission or emission from ST states, the undoped sample exhibits slightly larger amplitude of fast decaying components than that of the doped sample. At longer wavelengths, the amplitude of the slower decay becomes more prominent for the doped sample. It is quite evident from the decay traces that overall fluorescence lifetime increases noticeably as the wavelength is changed from 430 to 460 nm.

The individual wavelength decay traces were fit using multi-exponential fitting with the rise being fit by the instrument response function (IRF), as collected from a scattering sample. Each decay trace, which was both wavelength and delay window-dependent, was fit first with both lifetime and initial intensity as variable fitting parameters. The individual lifetime components were averaged, and each decay was refit with lifetime fixed and initial intensity as the variable parameter. This process was then reversed, and the traces were fit with initial intensity fixed and lifetime as the variable fitting parameter. The individual lifetime components were reaveraged, and the individual traces were again fit with initial intensity as the variable fitting parameter. As a result, one equation, $f(t)$, was established, which could describe the decay trace for any time window and any wavelength with initial intensity (A_1, A_2, ...) being the only variable parameter, with y accounting for baseline correction, reported as eq 1

$$f(t) = y + \sum A e^{t/\tau} \tag{1}$$

The time constants did not show any wavelength dependence over the observed wavelengths. On the time scale of 50 ns, the time-resolved PL decay profiles for both doped and undoped samples could be fit using the same multiexponential decay, yielding 1.1 ± 0.05 (τ_1) and 12 ± 1 ns (τ_2) time constants corresponding to the undoped sample and 1.0 ± 0.05 and 10 ± 1 ns for the doped sample (Table 1). Fitting the data taken on the longer time scale of 380 ns generates one more decay component with the lifetime varying from 60 ± 10 ns (τ_3) in undoped sample to 100 ± 10 ns in the doped sample. The residual plots corresponding to the fitting of different decay traces have been reported in the Supporting Information (Figures S3 and S4)

Emission collected between 430 and 460 nm derives mostly from the recombination of trap-state electrons. These electrons must decay through phonons and wait for a compatible nuclear configuration before they can recombine with hole. A perfect fitting in this region generates a fast component decaying within a few tens of picoseconds, which is ignored because it is on the same time scale as the instrumental resolution. The next fastest component with a lifetime of ~1 ns is attributed to the near band-edge emission or excitonic emission, whereas the lifetime of 10 ns is assigned to emission from ST states, which involve Zn dangling bonds. The slow decaying component (60 ns in undoped sample and 100 ns for the doped sample) probably corresponds to emission from DT states created by Se^{2-} dangling bonds or zinc vacancies or self-activated emission involving a DAP recombination, as previously reported for Mn^{2+}-doped sample.[49]

were investigated using the TCSPC technique. The charge carrier dynamics in doped and undoped ZnSe NCs was monitored following photoexcitation at 395 nm. Owing to the small Stokes shift (15–20 nm), the samples had to be excited with energy at least 15–20 nm higher than that needed for the first excitonic transition to eliminate laser scatter in the decay trace. This excitation energy was low enough to ensure that the first or lowest energy exciton was created and hot electron relaxation dynamics would be minimized. The samples did not show any sign of photobleaching during the course of measurements, which could otherwise introduce complications to the measurements.

The results, normalized by maximum amplitude, for time-resolved emission between 430 and 460 nm are shown in Figure 9, with time scales varying from the 50 ns range in Figure 9a,b to the 380 ns in Figure 9c. For the decay trace

H

dx.doi.org/10.1021/jp2047272 |*J. Phys. Chem. C* XXXX, XXX, 000–000
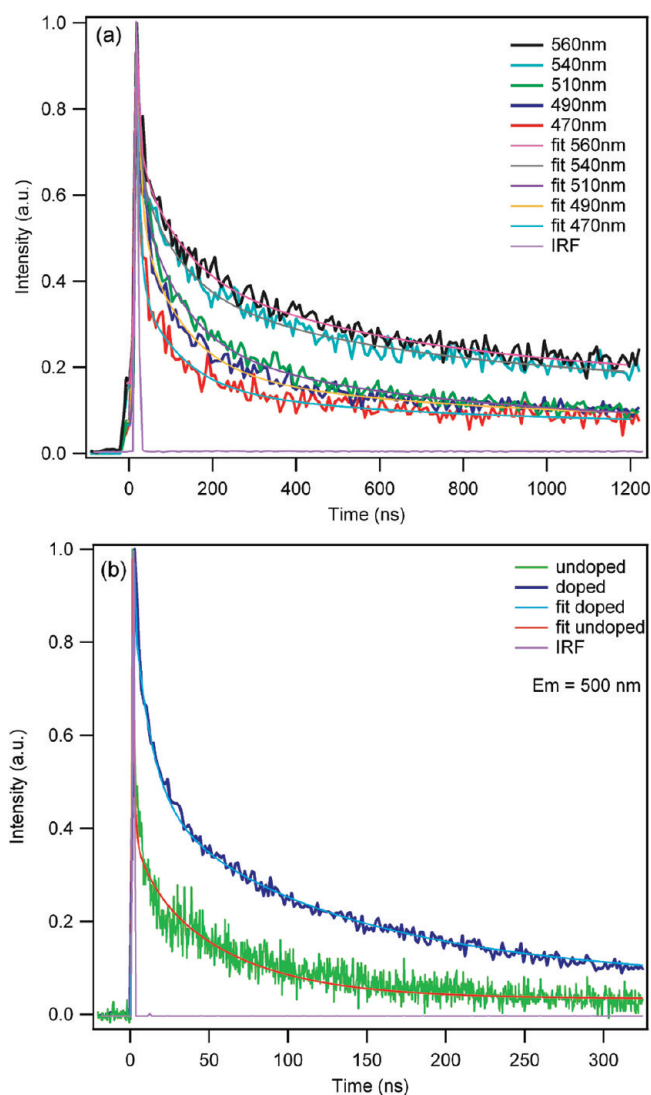
Figure 10. (a) Time-resolved emission decays of doped sample collected at 470, 490, 510, 530, and 560 nm. (b) 500 nm emission intensity versus time for undoped (green) and doped (red) samples.

Comparison of the time-resolved decay curves for the doped and undoped samples can provide insight about the origin of emission bands in the blue region along with the effect of doping on various decay components. Because the electrons residing in CB or ST states are delocalized, there would be a significant overlap between the electron and hole wave functions, which results in faster decay due to higher exciton recombination probability. In addition, interstitial and surface defect states could be partaken by these delocalized electrons that further increase the decay rate for this emission. Both of these factors justify why emission decay at 430 nm has a larger amplitude fast component than that observed for 460 nm emission, as shown in Figure 9. Similar to the reports in other systems like CdS and ZnS,[23,87,88] a definite correspondence has been observed between the emission wavelength and the decaying rate, where the emission decay is faster when it is closer to the bandedge. This is due to the reason that electrons/holes in the CB/VB or in ST states are more delocalized as compared with the charge carriers in DT states, which results in more overlap of electron and hole wave functions, leading to the faster decay.

The change in lifetime for DT state emission from 60 to 100 ns after doping is indicative of significant interaction between the dopant levels and DT states. This could be due to the reason that Cu^+, being relatively negatively charged with respect to the neighboring lattice, acts as an efficient hole trap center so that the hole trap states of the host lying closer to the VB like the Cu^+ state (Figure 6) can no longer trap the hole as effectively as in the case of undoped sample. This would result in DT state emission originating mostly from the hole trap states that are relatively deeper as compared with those involved in the case of undoped sample. With the hole trap states lying deeper in the doped system, there would be less overlap between the hole and electron wave functions due to the localization of deeper states which results in increasing the lifetime of DT state emission. A slight decrease in the lifetimes of short-lived components after doping suggests that the Cu dopant has some influence on the ST states as well. One possible mechanism is that the Cu dopant competes with the ST states in trapping the charge carriers from the CB or near-bandedge states. Alternatively, lifetime shortening could be due to the increased density of trap states caused by the Cu dopant in ZnSe host.

3.9.2. Kinetics of the Green Emission Band. Emission from DT states constitutes the PL in the region from ~430−630 nm for the undoped sample, whereas for the doped sample, Cu-related emission dominates in this region. Copper green emission, having maxima around 515 nm, has significant overlap from trap state emission, as indicated by the PL spectrum of the undoped sample (Figure 5), where the long tail of the near bandedge emission extends up to 570 nm. Therefore, the first half of the green emission band in the doped sample would have considerable contributions from ZnSe trap states in addition to the dopant emission. To characterize the effect of the decrease in the DT state emission on the decay profile, decay traces were collected at different wavelengths across the green emission band ranging from 470 to 560 nm, as shown in Figure 10a; however, data for the undoped sample were collected only up to 500 nm because of the low intensity at longer wavelengths.

Figure 10b shows the fluorescence decay collected at 500 nm for the doped and undoped samples. It is evident that the decay was faster in the undoped sample, and the long-lived component of doped sample was quite pronounced. The wavelength-dependent decay traces are reported in Figure 10a for the doped sample, which show that the amplitude of long-lived component becomes increasingly dominant at longer wavelengths.

A multiexponential fit to the decay profiles of the doped sample collected in this wavelength region yields a long-lived component with a lifetime of ~600 ± 130 ns. This slow decay component, present only in the doped sample, must be due to copper-related emission. Because the host peak in the doped sample was not completely eliminated, there might be some particles that were left undoped that could affect the relative amplitude of the decay components due to Cu versus trap states. However, this should not alter the kinetics of dopant or trap state emission.

The percent contribution by each lifetime component to the overall fluorescence process was calculated for each decay profile of the series of wavelengths observed (Figure S5 of the Supporting Information). For calculation of percent contribution, each wavelength-dependent fitting function, which had only the initial intensity as the variable and was the sum of all individual lifetime components $f(t)$ (eq 1), was integrated and compared with the integrated intensity for each individual component, an example of
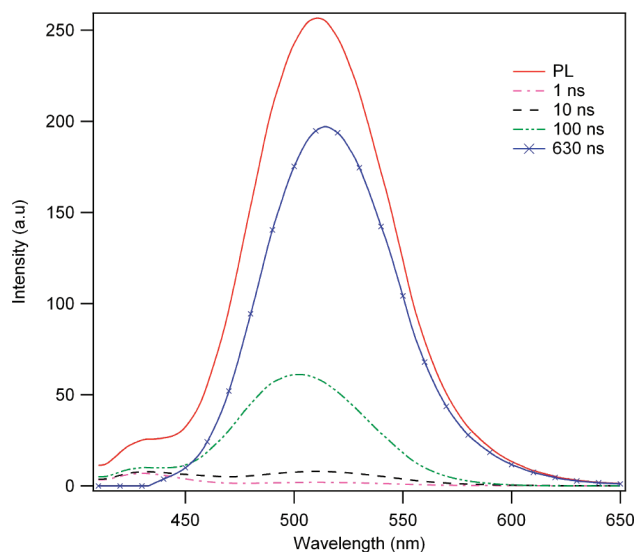
I

dx.doi.org/10.1021/jp2047272 |*J. Phys. Chem. C* XXXX, XXX, 000–000

Figure 11. Spectral deconvolution indicating the contribution of various components to the time-integrated PL spectrum.

which is reported in eq 2. This was taken to be the percent contribution from that lifetime component at a specific wavelength.

$$\% \text{ intensity } (\lambda) = \frac{\int A_1 e^{-t/\tau_1} \, dt}{\int f(t) \, dt} * 100 \qquad (2)$$

Fitting the data in Figure S5 of the Supporting Information, the intensity was calculated over the entire PL spectral range for each lifetime component. Subsequently, these data were used to deconvolve the PL spectrum, as shown in Figure 11. This plot clearly indicates that the majority of the emitted photons coming from the doped sample are due to the Cu impurity. There is still a large portion of the photons coming from DT state emission; however, it is interesting to note that this component has a maxima at relatively longer wavelength (500 nm), as compared with that of undoped sample (478 nm). This observation further supports the argument for increase in lifetime of DT states after doping.

As previously mentioned, in the case of Cu green emission, excitation of a VB electron to the CB is followed by the formation of a transient Cu^{2+} acceptor. The subsequent capture of the electron by this acceptor is expected to be slow because of the low electron capture cross section of Cu^{2+}.[89] At room temperature, the lifetime for Cu dopant in ZnS has been reported to be 500 ns,[67] whereas in this study, it is longer (630 ns) but nevertheless very close. The difference in lifetimes observed for ZnSe:Cu and ZnS:Cu may be partially due to different energetics of ZnSe as compared with ZnS including bandgap location and bandgap energy but could also be due to variability in the nonradiative recombination pathways. Also, in the same work by Bol et al., the Cu lifetime at 4 K was reported to be 20 μs. Because the quantum yield was measured to be 2 to 3% in this study, the radiative component was calculated to be 25 $\pm$ 5 μs, which is in agreement with the low-temperature studies. The long-lived radiative component is very similar to that of the triplet state emission observed in Cu^+-doped glasses at room temperature, which was measured to be 41 μs.[90] It is, therefore, likely that the dopant emission in these systems involves a triplet as well; however, direct evidence of this has not been reported.

At longer wavelengths, it was expected that the major decay process contributing to emission would be coming from energy exchange to the Cu phosphor. This is also clear from the trend that relative ratio of amplitudes of fast components to that of slow components decreases as the emission wavelength is moved from the left-hand side of the dopant peak to the right-hand side (Figure 10a). However, this decrease in amplitude ratio that is due to decreasing overlap of trap state emission with dopant emission (Figure 5) does not affect the time constant for slow decay component due to copper.

4. CONCLUSIONS

Stable Cu-doped ZnSe NCs were prepared using ODA as a capping agent. Adding the dopant at a stage where host NCs have developed well-defined crystal facets helped to adsorb copper strongly on to the NCs that would not be expelled onto the surface when ZnSe shell is grown. After solvent extractions to remove the unreacted precursors, NCs stored in a mixture of hexanes and ODE are very stable and demonstrate quantum yield up to 3−8% even after months. Cu doping introduces efficient hole traps that quench the emission involving hole trap states lying closer to the VB and significantly increases the lifetime of DT states probably due to decreased coupling in electron and hole trap states comprising DT state emission. In addition, Cu doping slightly decreases the lifetimes of fast decay components arising from excitonic and ST state emissions by competing with these states in trapping the charge carriers. The EXAFS results indicate that in the NC samples used for the EXAFS studies many of the Cu neighbors are O atoms. This might arise from Cu mainly on or close to the NC surface. It is interesting that Cu appears to have four neighbors in ZnSe and the Cu−Se bond length is close to the expected value because for ZnS:Cu at low concentrations the number of S neighbors is closer to 3, and the Cu−S bond is compressed. The doping approach adopted is successful in preparing stable Cu-doped semiconductor NCs, and time-resolved PL studies of the charge carrier dynamics is helpful in understanding their fundamental optical and electronic properties in relation to their structural characteristics revealed by EXAFS and other techniques.

■ ASSOCIATED CONTENT

⑤ Supporting Information. EPR spectra of ZnSe:$Cu_{0.5\%}$ and reference copper acetate sample; UV−visible absorption spectra of an undoped and a representative doped sample; residual plots corresponding to the fitting of decay traces collected at 430 and 460 nm (Figure 9); residual plots corresponding to the fitting of decay traces shown in Figure 10; and plots showing the percent contribution of different lifetime components to the time-integrated PL spectrum of the doped sample. This material is available free of charge via the Internet at http://pubs.acs.org.

■ AUTHOR INFORMATION

Corresponding Author
*E-mail: zhang@ucsc.edu.

■ ACKNOWLEDGMENT

J

dx.doi.org/10.1021/jp2047272 |*J. Phys. Chem. C* XXXX, XXX, 000–000

■ REFERENCES

(1) Klimov, V. I.; Ivanov, S. A.; Nanda, J.; Achermann, M.; Bezel, I.; McGuire, J. A.; Piryatinski, A. *Nature* **2007**, *447*, 441.

(2) Burda, C.; Chen, X.; Narayanan, R.; El-Sayed, M. A. *Chem. Rev.* **2005**, *105*, 1025.

(3) Shim, M.; Wang, C.; Guyot-Sionnest, P. *J. Phys. Chem. B* **2001**, *105*, 2369.

(4) Chan, W. C. W.; Nie, S. *Science* **1998**, *281*, 2016.

(5) Chen, C. C.; Herhold, A. B.; Johnson, C. S.; Alivisatos, A. P. *Science* **1997**, *276*, 398.

(6) Nirmal, M.; Dabbousi, B. O.; Bawendi, M. G.; Macklin, J. J.; Trautman, J. K.; Harris, T. D.; Brus, L. E. *Nature* **1996**, *383*, 802.

(7) Alivisatos, A. P. *Science* **1996**, *271*, 933.

(8) Brus, L. E. *J. Chem. Phys.* **1983**, *79*, 5566.

(9) Murray, C. B.; Norris, D. J.; Bawendi, M. G. *J. Am. Chem. Soc.* **1993**, *115*, 8706.

(10) Pradhan, N.; Battaglia, D. M.; Liu, Y.; Peng, X. *Nano Lett.* **2007**, *7*, 312.

(11) Alivisatos, P. *Nat. Biotechnol.* **2003**, *22*, 47.

(12) Colvin, V. L.; Schlamp, M. C.; Alivisatos, A. P. *Nature* **1994**, *370*, 354.

(13) Nozik, A. J. *Annu. Rev. Phys. Chem.* **2001**, *52*, 193–231.

(14) Michalet, X.; Pinaud, F.; Bentolila, L.; Tsay, J.; Doose, S.; Li, J.; Sundaresan, G.; Wu, A.; Gambhir, S.; Weiss, S. *Science* **2005**, *307*, 538.

(15) Gur, I.; Fromer, N. A.; Geier, M. L.; Alivisatos, A. P. *Science* **2005**, *310*, 462.

(16) Bruchez, M., Jr; Moronne, M.; Gin, P.; Weiss, S.; Alivisatos, A. P. *Science* **1998**, *281*, 2013.

(17) Derfus, A. M.; Chan, W. C. W.; Bhatia, S. N. *Nano Lett.* **2004**, *4*, 11.

(18) Meulenberg, R. W.; van Buuren, T.; Hanif, K. M.; Willey, T. M.; Strouse, G. F.; Terminello, L. J. *Nano Lett.* **2004**, *4*, 2277.

(19) Wang, F.; Liu, X. *J. Am. Chem. Soc.* **2008**, *130*, 5642.

(20) Yu, J. H.; Liu, X.; Kweon, K. E.; Joo, J.; Park, J.; Ko, K. T.; Lee, D. W.; Shen, S.; Tivakornsasithorn, K.; Son, J. S. *Nat. Mater.* **2010**, *9*, 47.

(21) Chen, W.; Zhang, J. Z.; Joly, A. G. *J. Nanosci. Nanotechnol.* **2004**, *4*, 919.

(22) Bhargava, R.; Gallagher, D.; Hong, X.; Nurmikko, A. *Phys. Rev. Lett.* **1994**, *72*, 416.

(23) Smith, B. A.; Zhang, J. Z.; Joly, A.; Liu, J. *Phys. Rev. B* **2000**, *62*, 2021.

(24) Schwartz, D. A.; Norberg, N. S.; Nguyen, Q. P.; Parker, J. M.; Gamelin, D. R. *J. Am. Chem. Soc.* **2003**, *125*, 13205.

(25) Pradhan, N.; Goorskey, D.; Thessing, J.; Peng, X. *J. Am. Chem. Soc.* **2005**, *127*, 17586.

(26) Bhargava, R. N.; Gallagher, D.; Hong, X.; Nurmikko, A. *Phys. Rev. Lett.* **1994**, *72*, 416.

(27) Sooklal, K.; Cullum, B. S.; Angel, S. M.; Murphy, C. J. *J. Phys. Chem.* **1996**, *100*, 4551.

(28) Norris, D. J.; Yao, N.; Charnock, F. T.; Kennedy, T. A. *Nano Lett.* **2001**, *1*, 3.

(29) Erwin, S. C.; Zu, L.; Haftel, M. I.; Efros, A. L.; Kennedy, T. A.; Norris, D. J. *Nature* **2005**, *436*, 91.

(30) Mikulec, F. V.; Kuno, M.; Bennati, M.; Hall, D. A.; Griffin, R. G.; Bawendi, M. G. *J. Am. Chem. Soc.* **2000**, *122*, 2532.

(31) Pradhan, N.; Peng, X. *J. Am. Chem. Soc.* **2007**, *129*, 3339.

(32) Norris, D.; Yao, N.; Charnock, F.; Kennedy, T. *Nano Lett.* **2001**, *1*, 3.

(33) Jana, S.; Srivastava, B. B.; Acharya, S.; Santra, P. K.; Jana, N. R.; Sarma, D.; Pradhan, N. *Chem. Commun.* **2010**, *46*, 2853.

(34) Li, S. S.; Liu, F. T.; Wang, Q.; Chen, X. X.; Yang, P. *Adv. Mater. Res.* **2009**, *79*, 2043.

(35) Mittleman, D. M.; Schoenlein, R. W.; Shiang, J. J.; Colvin, V. L.; Alivisatos, A. P.; Shank, C. V. *Phys. Rev. B* **1994**, *49*, 14435.

(36) Jones, M.; Lo, S. S.; Scholes, G. D. *J. Phys. Chem. C* **2009**, *113*, 18632.

(37) Wise, F. W. *Acc. Chem. Res.* **2000**, *33*, 773.

(38) Dubertret, B.; Skourides, P.; Norris, D. J.; Noireaux, V.; Brivanlou, A. H.; Libchaber, A. *Science* **2002**, *298*, 1759.

(39) Žutic, I.; Fabian, J.; Sarma, S. D. *Rev. Mod. Phys.* **2004**, *76*, 323.

(40) Seth Coe, W. K. W.; Moungi Bawendi, V. B. *Nature* **2002**, *420*, 800.

(41) Scholes, G. D.; Rumbles, G. *Nat. Mater.* **2006**, *5*, 683.

(42) Klimov, V. I. *J. Phys. Chem. B* **2000**, *104*, 6112.

(43) Scholes, G. D. *ACS Nano* **2008**, *2*, 523.

(44) Kippeny, T. C.; Bowers, M. J.; Dukes Iii, A. D.; McBride, J. R.; Orndorff, R. L.; Garrett, M. D.; Rosenthal, S. J. *J. Chem. Phys.* **2008**, *128*, 084713.

(45) Zhang, J. Z. *Acc. Chem. Res.* **1997**, *30*, 423.

(46) Skinner, D. E.; Colombo, D. P.; Cavaleri, J. J.; Bowman, R. M. *J. Phys. Chem.* **1995**, *99*, 7853.

(47) Olano, E. M.; Grant, C. D.; Norman, T. J.; Castner, E. W.; Zhang, J. Z. *J. Nanosci. Nanotechnol.* **2005**, *5*, 1492.

(48) Fang, Z.; Wu, P.; Zhong, X.; Yang, Y. J. *Nanotechnology* **2010**, *21*, 305604.

(49) Gan, C.; Zhang, Y.; Battaglia, D.; Peng, X.; Xiao, M. *Appl. Phys. Lett.* **2008**, *92*, 241111.

(50) Peng, X.; Wickham, J.; Alivisatos, A. *J. Am. Chem. Soc.* **1998**, *120*, 5343.

(51) Qu, L.; Peng, X. *J. Am. Chem. Soc.* **2002**, *124*, 2049.

(52) Booth, C. H. *R-Space X-ray Absorption Package*; Lawrence National Laboratory: Berkeley, CA, 2005.

(53) Becker, W. *Advanced Time-Correlated Single Photon Counting Techniques*; Springer: Berlin, 2005.

(54) Yu, W. W.; Wang, Y. A.; Peng, X. *Chem. Mater.* **2003**, *15*, 4300.

(55) Battaglia, D.; Peng, X. *Nano Lett.* **2002**, *2*, 1027.

(56) Yu, W. W.; Peng, X. *Angew. Chem.* **2002**, *114*, 2474.

(57) Mikulec, F. V.; Kuno, M.; Bennati, M.; Hall, D. A.; Griffin, R. G.; Bawendi, M. G. *J. Am. Chem. Soc.* **2000**, *122*, 2532.

(58) Dalpian, G. M.; Chelikowsky, J. R. *Phys. Rev. Lett.* **2006**, *96*, 226802.

(59) Shiang, J. J.; Kadavanich, A. V.; Grubbs, R. K.; Alivisatos, A. P. *J. Phys. Chem.* **1996**, *100*, 13886.

(60) Kaelble, E. F. *Handbook of X-rays*; McGraw Hill: New York, 1967.

(61) Ankudinov, A. L.; Ravel, B.; Rehr, J. J.; Conradson, S. D. *Phys. Rev. B* **1998**, *58*, 7565.

(62) Katari, J. E. B.; Colvin, V.; Alivisatos, A. *J. Phys. Chem.* **1994**, *98*, 4109.

(63) Norman, T. J.; Magana, D.; Wilson, T.; Burns, C.; Zhang, J. Z.; Cao, D.; Bridges, F. *J. Phys. Chem. B* **2003**, *107*, 6309.

(64) Corrado, C.; Jiang, Y.; Oba, F.; Kozina, M.; Bridges, F.; Zhang, J. Z. *J. Phys. Chem. A* **2009**, *113*, 3830.

(65) Segal, L.; Eggerton, F. V. *Appl. Spectrosc.* **1961**, *15*, 112.

(66) Wang, Q.; Liu, F. T.; Jiang, Q. H.; Chen, X. X.; Wang, D. Z. *Adv. Mater. Res.* **2011**, *148*, 1268.

(67) Bol, A. A.; Ferwerda, J.; Bergwerff, J. A.; Meijerink, A. *J. Lumin.* **2002**, *99*, 325.

(68) Tang, A.; Yi, L.; Han, W.; Teng, F.; Wang, Y.; Hou, Y.; Gao, M. *Appl. Phys. Lett.* **2010**, *97*, 033112.

(69) Isarov, A. V.; Chrysochoos, J. *Langmuir* **1997**, *13*, 3142.

(70) Bowers, R.; Melamed, N. *Phys. Rev.* **1955**, *99*, 1781.

(71) Srivastava, B. B.; Jana, S.; Pradhan, N. *J. Am. Chem. Soc.* **2011**, *133*, 1007.

K

dx.doi.org/10.1021/jp2047272 |*J. Phys. Chem. C* XXXX, XXX, 000–000

(72) Holton, W.; De Wit, M.; Watts, R.; Estle, T.; Schneider, J. *J. Phys. Chem. Solids* **1969**, *30*, 963.

(73) *Semiconductors-Basic Data*, 2nd ed.; Springer: Berlin, 1996.

(74) Dunstan, D. J.; Cavenett, B. C.; Brunwin, R. F.; Nicholls, J. E. *J. Phys. C: Solid State Phys.* **1977**, *10*, L361.

(75) Iida, S. *J. Phys. Soc. Jpn.* **1968**, *25*, 177.

(76) Godlewski, M.; Lamb, W.; Cavenett, B. *Solid State Commun.* **1981**, *39*, 595.

(77) Jones, G.; Woods, J. *J. Lumin.* **1974**, *9*, 389.

(78) Morozova, N.; Karetnikov, I.; Blinov, V.; Gavrishchuk, E. *Semiconductors* **2001**, *35*, 24.

(79) Stringfellow, G. B.; Bube, R. H. *J. Appl. Phys.* **1968**, *39*, 3657.

(80) Dunstan, D.; Nicholls, J.; Cavenett, B.; Davies, J. *J. Phys. C: Solid State Phys.* **1980**, *13*, 6409.

(81) Ivanova, G.; Kasiyan, V.; Nedeoglo, D.; Oprya, S. *Semiconductors* **1998**, *32*, 154.

(82) Pokrant, S.; Whaley, K. *Eur. Phys. J. D* **1999**, *6*, 255.

(83) Underwood, D. F.; Kippeny, T.; Rosenthal, S. J. *J. Phys. Chem. B* **2001**, *105*, 436.

(84) Godlewski, M.; Lamb, W.; Cavenett, B. *J. Lumin.* **1981**, *24*, 173.

(85) Peka, P.; Schulz, H. J. *Solid State Commun.* **1994**, *89*, 225.

(86) Heitz, R.; Hoffmann, A.; Thurian, P.; Broser, I. *J. Phys.: Condens. Matter* **1992**, *4*, 157.

(87) O'Neil, M.; Marohn, J.; McLendon, G. *Chem. Phys. Lett.* **1990**, *168*, 208.

(88) Roberti, T. W.; Cherepy, N. J.; Zhang, J. Z. *J. Chem. Phys.* **1998**, *108*, 2143.

(89) Hemila, S. O.; Bube, R. H. *J. Appl. Phys.* **1967**, *38*, 5258.

(90) Debnath, R.; Chaudhury, J.; Bera, S. C. *Phys. Status Solidi B* **1990**, *157*, 723.